



BIREFRINGENT DIRAC FERMION IN ANISOTROPIC VELOCITY  
MODULATED GRAPHENE JUNCTION

MR. EAKKARAT PATTRAWUTTHIWONG

A THESIS SUBMITTED IN PARTIAL FULFILLMENT OF THE REQUIREMENTS  
FOR THE DEGREE OF MASTER OF SCIENCE (PHYSICS)  
FACULTY OF SCIENCE  
KING MONGKUT'S UNIVERSITY OF TECHNOLOGY THONBURI  
2020

Electronic Transport of Dirac Fermion in Tilted Velocity Modulated Dirac  
Material Junction

Mr. Eakkarat Pattrawutthiwong B.Sc. (Applied Physics)

A Thesis Submitted in Partial Fulfillment of the Requirements for  
the Degree of Master of Science (Physics)

Faculty of Science

King Mongkut's University of Technology Thonburi

2020

Thesis Committee

..... Chairman of Thesis Committee  
(Asst. Prof. Thana Sutthibutpong, Ph.D.)

..... Member and Thesis Advisor  
(Asst. Prof. Watchara Liewrian, Ph.D.)

..... Member  
(Tanapat Deesuwan, Ph.D.)

..... Member  
(Suwat Tangwancharoen, Ph.D.)

Copyright reserved

Thesis Title      Electronic Transport of Dirac Fermion in Tilted Velocity  
Modulated Dirac Material Junction

Thesis Credits    12

Candidate        Mr. Eakkarat Patrawutthiwong

Thesis Advisor    Asst. Prof. Watchara Liewrian

Program          Master of Science

Field of Study    Physics

Department       Physics

Faculty           Science

Academic Year    2020

### Abstract

The ground state entanglement of the system, both in discrete-time and continuous-time cases, is quantified through the linear entropy. The result shows that the entanglement increases as the interaction between the particles increases in both time scales. It is also found that the strength of the harmonic potential affects the entanglement of the system. The different feature of the entanglement between continuous-time and discrete-time scales is that, for discrete-time entanglement, there is a cut-off condition. This condition implies that the system can never be in a maximally entangled state.

Keywords : Continuous-Time/ Discrete-Time/ Entanglement

## **ACKNOWLEDGEMENTS**

This thesis is supported by my thesis advisor, Dr. Monsit Tanasittikosol for editing and supporting my thesis writing. Next, I would like to thank another advisor, Asst. Prof. Dr for invaluable teaching and giving the motivation in my thesis. Without their advices, this thesis would not have been completed.

## CONTENTS

	<b>PAGE</b>
<b>ABSTRACT IN ENGLISH</b>	ii
<b>ACKNOWLEDGMENTS</b>	iii
<b>CONTENTS</b>	iv
<b>LIST OF FIGURES</b>	vi
<b>CHAPTER</b>	
<b>1. INTRODUCTION</b>	<b>1</b>
1.1 Background and motivation . . . . .	1
<b>2. THEORETICAL BACKGROUND</b>	<b>2</b>
2.1 Klein tunneling effect . . . . .	2
2.2 Electronic transport of electron in graphene under the influence of magnetic field . . . . .	4
2.3 Asymmetric tunneling of electron in tilted Weyl cone systems . . . . .	4
<b>3. MODEL AND METHOD</b>	<b>9</b>
3.1 Field-Effect transistor . . . . .	9
3.2 Transmission probability of electron in tilted Dirac cone . . . . .	10
3.3 The elliptic Fermi surface of tilted Dirac cone . . . . .	12
3.4 Angular dependent wavevector of tilted Dirac cone . . . . .	12

	PAGE
<b>4. RESULT AND DISCUSSION</b>	<b>14</b>
4.1 Angular dependent of transmission probability . . . . .	14
4.2 The tilted strength identification by means of the tunneling resonance properties . . . . .	15
4.3 Oscillatory behavior of electron resonant tunneling . . . . .	16
4.4 Revisit: The tilted strength identification by means of the tunneling resonance properties . . . . .	17
4.5 Pseudo magnetic field . . . . .	19
4.6 The key consequence of the mismatch effect . . . . .	19
4.7 Transmission under the influence of pseudo magnetic field . . . . .	21
<b>5. CONCLUSION</b>	<b>23</b>
<b>REFERENCES</b>	<b>25</b>
<b>BIOGRAPHY</b>	<b>26</b>

## LIST OF FIGURES

<b>FIGURE</b>		<b>PAGE</b>
2.1 Schematic diagram of electron propagation through the potential barrier of height $V_0$ and width $D$ . . . . .		2
2.2 The transmission probability as a function of incident angle with different barrier height. $V_0 = 200$ meV for red curve and 285 meV for blue curve [4]. . . . .		4
2.3 transistor . . . . .		5
2.4 anomalous tunneling . . . . .		7
2.5 anomalous Fermi surfaces . . . . .		8
3.1 Schematic illustration of Dirac material n-p-n heterojunctions with the mismatch of Dirac cone. The position of Fermi energy level $E_F$ can be controlled by tuning the voltage through potential gate of length $L$ . . . . .		10
4.1 The same cup of coffee. Two times. . . . .		15
4.2 tp fixed angle . . . . .		17
4.3 (a) The device structure for the measurement of resonant tunneling electron. Straight blue lines represent the transport region where both arms are $45^\circ$ angled with the normal direction. Green and yellow region represents top gate and electrode respectively. (b) Angular-dependent transmission for different applied voltages, $U=180.2$ meV for solid line and $U=185.85$ meV for dashed-dotted line. These voltages satisfy the resonance condition at $\phi = \frac{\pi}{4}$ . . . . .		18



# **CHAPTER 1 INTRODUCTION**

## **1.1 Background and motivation**

The electronic properties of material are defined by the ability of charge carriers to move throughout the crystal structures

The ability of charge carriers to tunnel throughout the material is defines by the crystal, electronic structures of their host material.

## CHAPTER 2 THEORETICAL BACKGROUND

### 2.1 Klein tunneling effect

Klein tunneling refers to a relativistic particles penetrate through the potential barrier without backscattering. These properties was once unique to the high-energy particles, where it can only be observed in the system with high-driven voltage. In 2006, this effect is predicted to occur in low-energy system of graphene [4]. This is because the electron in graphene mimics the relativistic massless Dirac particle and obey massless Dirac equation

$$\hat{H} = -i\hbar v_F \sigma \nabla \quad (2.1)$$

where  $v_F \approx 10^6 \text{ ms}^{-1}$  is Fermi velocity,  $\sigma = (\sigma_x, \sigma_y)$  is Pauli matrix.

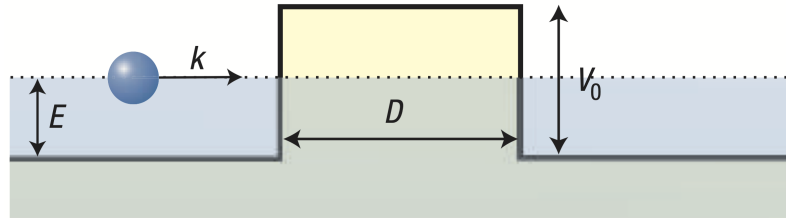


**Figure 2.1** Schematic diagram of electron propagation through the potential barrier of height  $V_0$  and width  $D$

The electron propagation can be modeled as in Fig. 2.1, consisting of three transport regions where the Fermi energy of electron is below the potential barrier. By solving

Eq. 2.1, the wave function of each region can be expressed as follows

$$\psi_1 = \begin{cases} (e^{ik_xx} + re^{-ik_xx})e^{ik_yy}, & x < 0, \\ (ae^{iq_xx} + be^{-iq_xx})e^{ik_yy}, & 0 < x < D, \\ te^{ik_xx+ik_yy}, & x > D, \end{cases} \quad (2.2)$$

$$\psi_2 = \begin{cases} s(e^{ik_xx+i\phi} - re^{-ik_xx-i\phi})e^{ik_yy}, & x < 0, \\ s'(ae^{iq_xx+i\theta} - be^{-iq_xx-i\theta})e^{ik_yy}, & 0 < x < D, \\ st e^{ik_xx+ik_yy+i\phi}, & x > D, \end{cases}$$

where  $k_x = k \cos \phi$  and  $k_y = k \sin \phi$  are x- and y-component wavevector outside the barrier region, respectively.  $q_x = \sqrt{(E - V_0)^2 / (\hbar v_F)^2 - k_y^2}$  is x-component wavevector inside the barrier region.  $s = \text{sgn}(E)$  and  $s' = \text{sgn}(E - V_0)$ . Since the wave function of each region has to be continuous at the boundary, we can substitute  $x = 0$  and  $x = D$  to Eq. 2.2, which give

$$\begin{aligned} 1 + r - a - b &= 0 \\ s(e^{i\phi} - e^{-i\phi}r) - s'(e^{i\theta}a - e^{-i\theta}b) &= 0 \\ e^{iDq_x}a + e^{-iDq_x}b - e^{iDk_x}t &= 0 \\ s'(e^{iDq_x+i\theta}a - e^{-iDq_x-i\theta}b) - se^{iDk_x+i\phi}t &= 0 \end{aligned} \quad (2.3)$$

where r and t is the reflection and transmission coefficient, respectively. Which can be obtained by solving the system of equations above. The reflection coefficient has the following expression

$$r = 2ie^{i\phi} \sin(q_x D) \times \frac{\sin \phi - ss' \sin \theta}{ss'[e^{-iq_x D} \cos(\phi + \theta) + e^{iq_x D} \cos(\phi - \theta)] - 2i \sin(q_x D)} \quad (2.4)$$

Since  $T = |t|^2 = 1 - |r|^2$ , the transmission probability can be expressed as follow

$$T = \frac{\cos^2 \phi}{1 - \cos^2 q_x D \sin^2 \phi} \quad (2.5)$$

Fig. 2.2 shows the polar plot of Eq. 2.5. At the incident angle  $\phi = 0$ , electron tunnels through the barrier with probability of one no matter the height of the potential barrier. This is the feature unique to massless Dirac fermion called Klein tunneling.

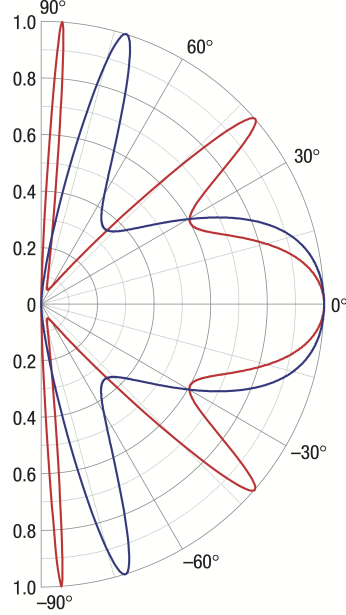


**Figure 2.2** The transmission probability as a function of incident angle with different barrier height.  $V_0 = 200$  meV for red curve and 285 meV for blue curve [4].

## 2.2 Electronic transport of electron in graphene under the influence of magnetic field

## 2.3 Asymmetric tunneling of electron in tilted Weyl cone systems

The electronic structure of pristine graphene is often symmetric and non-tilted, which indicate that the transmission of electron is symmetric with respect to normal incident angle as shown in section 2.1. Unlike the Dirac cone of graphene, in 3-dimensional Weyl semimetals, the Weyl cone around the Weyl point is generally tilted and anisotropic as Weyl points are not located on high-symmetry k-points. A tilted Weyl fermion can be described by the low energy Weyl Hamiltonian with asymmetric velocities

$$H = V_0 + \sum_i \hbar k_i (\sigma^i v_i + w_i) \quad (2.6)$$

where  $\sigma^i$  are the Pauli matrices,  $v_i$  are the velocities in 3 dimensions, and  $V_0$  is the potential barrier height.  $w_i$  is the tilt of Weyl cone in the unit of velocity. The model of interest is shown in Fig. 2.3 with the potential profile  $V_{(x)} = V_0[\Theta(x) - \Theta(x - L)]$ .

By solving the Hamiltonian above, the components of the wave functions are written as

$$\psi_{\pm} = \frac{1}{\sqrt{2}} e^{ik \rightarrow r \rightarrow} \begin{pmatrix} 1 \\ e^{i\phi} \sec \gamma (\pm 1 + \sin \gamma) \end{pmatrix} = \begin{pmatrix} \psi_a \\ \psi_b^{\pm} \end{pmatrix} \quad (2.7)$$

The transmission probability can be calculated by matching both components of the wave functions at the interfaces. The wave vector outside the potential barrier is expressed as

$$\begin{aligned} k_x &= k_F \cos \gamma \cos \phi, \\ k_y &= k_F \cos \gamma \sin \phi, \\ k_z &= k_F \sin \gamma \end{aligned} \quad (2.8)$$

and wave vector inside the potential barrier is

$$q_x = \frac{\sqrt{(E_F - V_0 - \hbar k_y w_y)^2 - \hbar^2 v_F^2 (k_y^2 + k_z^2)}}{\hbar v_F}. \quad (2.9)$$

The angles of electron propagation inside the potential barrier

$$\begin{aligned} \theta &= \arctan \left( \frac{k_y}{q_x} \right), \\ \alpha &= \arctan \left( \frac{k_z}{q_x} \cos \theta \right). \end{aligned} \quad (2.10)$$

can be calculated by considering the conservation of the transverse wave vectors  $k_y$  and  $k_z$  at the barrier interface  $x = 0$ .

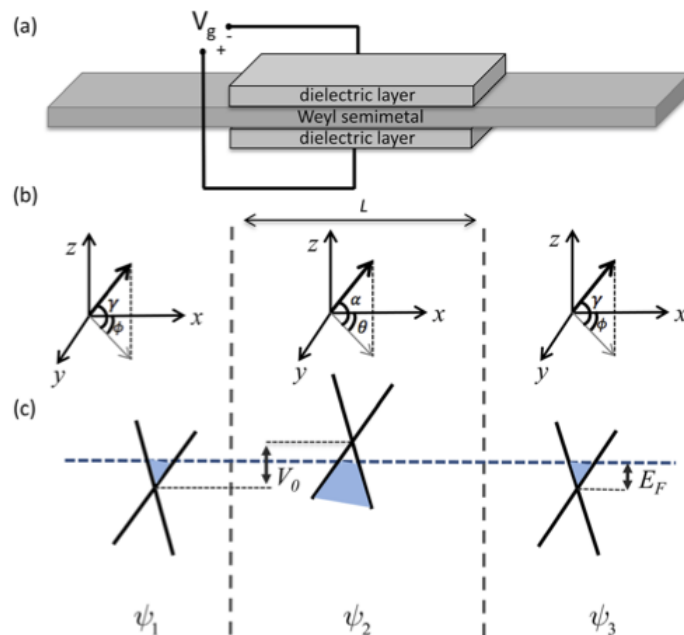


**Figure 2.3** transistor

In the case of non-tilted Weyl cone system, the transmission probability is symmetric with respect to  $\phi = 0$  and  $\gamma = 0$  as shown in Fig. 2.4a. Which similar to the transmission of electron in graphene except that it is confined to two dimensions, whereas the Weyl semimetal is three dimensions. This symmetric transmission becomes asymmetric when the Weyl cone is tilted along one of the transverse directions as shown in Fig. 2.4b. In other word, the transmission is shifted to the direction of the tilt. This can be understood by considering the Fermi surfaces in Fig. 2.5. In the case of  $\phi > \phi_{a,b}$ ,  $q_x$  becomes imaginary and the electron is totally reflected. The shaded angles show the allowed range where the electron can propagate through the barrier. The analytical form of the critical angle of incident electron is found as

$$\phi_a = \sin^{-1} \left( -\frac{v_F(V_0 - E_F)}{E_F v_F - V_0 w_y} \right) \quad (2.11)$$

In the previous studies, the asymmetric transmission was only analyzed in the system with step magnetic or strain gauge potential [5, 2, 10]. Fig. 2.5b shows the Fermi surface under the influence of magnetic step vector potential  $A_y = B_0 l_B \Theta(x) \hat{y}$ , where  $l_B = \sqrt{\frac{\hbar}{|e|B_0}}$ , which was shifted by the amount of  $k_y = k_y + \delta k_B$ . In this case, the critical angle of incident electron is found as

$$\phi_b = \sin^2 \left( -\frac{V_0 - E_F + \eta v_F \sqrt{|B_0 \hbar e|}}{E_F} \right) \quad (2.12)$$

where  $\eta = \text{sign}(B_z)$ . The equivalent y-component wavevector shifted due to the tilted Weyl cone and potential barrier can be approximately derived by considering the average of shift at the maximum and minimum points of  $k_y$ . By equating Eq. 2.11 and 2.12, the delta function pseudo-magnetic field generated by the application of potential barrier and tilted Weyl cone is given By

$$B \approx \frac{V_0^2 w_y^2}{e \hbar (w_y^2 - v_F^2)^2} \quad (2.13)$$

The transmission under the influence of magnetic vector potential is shown in Fig. 2.4f, where the magnetic field strength is calculated by Eq. 2.13 for  $V_0 = 160$  meV and  $w_y = 0.1 v_F$ . The result almost identical to those of the tilted Weyl semimetal without the magnetic barrier (see Fig. 2.4b).

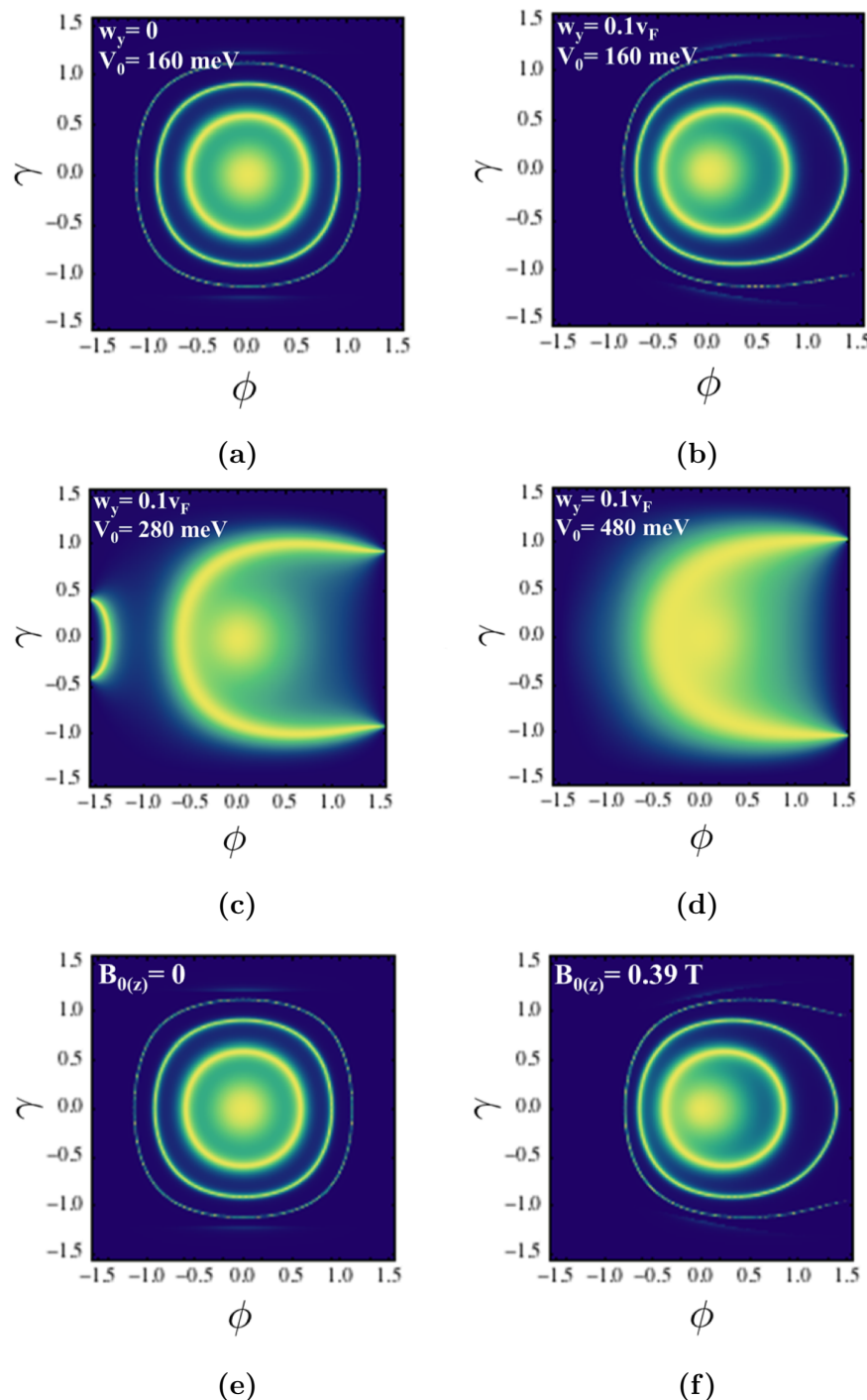


**Figure 2.4** anomalous tunneling

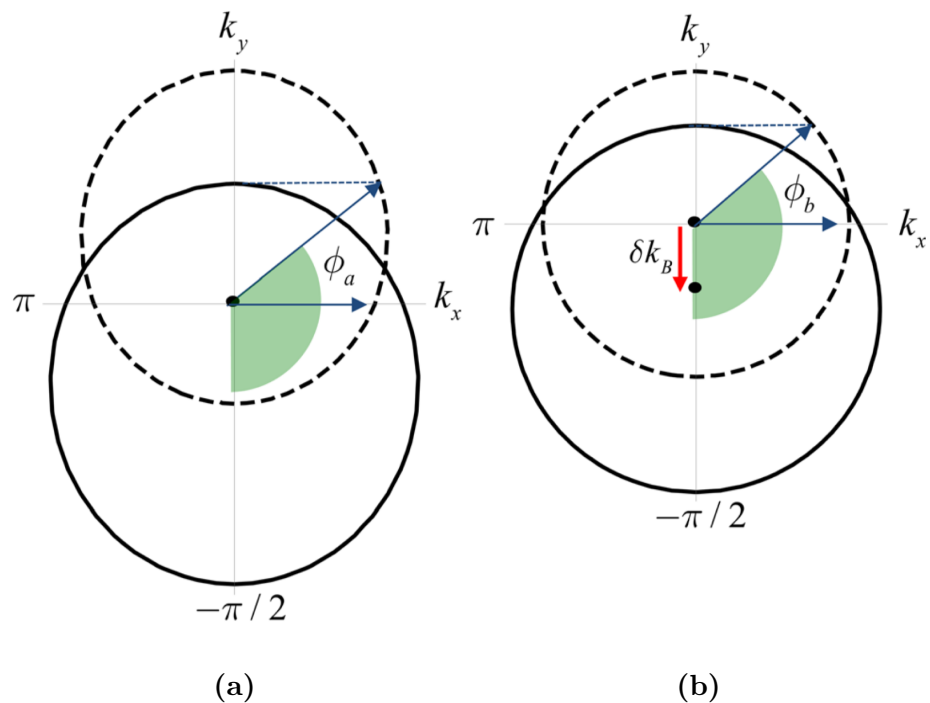


**Figure 2.5** anomalous Fermi surfaces

## CHAPTER 3 MODEL AND METHOD

In this work, the tunneling properties of electrons across the mismatch of the tilted Dirac cone are investigated. We assume that the electron propagations are coherent and not affected by ohmic contact due to the heterogeneity of the junctions. The tunneling properties considered here are in low energy limit, in which the inter-valley scattering between  $K$  and  $K'$  in the Brillouin zone is negligible [1]

### 3.1 Field-Effect transistor

The proposed structure is depicted in Fig. 3.1, consisting of 2-dimensional Dirac material n-p-n heterojunctions with different tilted Dirac cones. To achieve such a device structure, the top gate is placed in the middle region of length  $L$  to tune the Fermi energy level, which can be realized by depositing Ti/Au using standard electron beam lithography [3]. Electrostatic doping using the ionic-liquid gate also has been demonstrated, which enhanced the carrier mobility [6]. For the barrier profile, we use rectangular potential barrier.

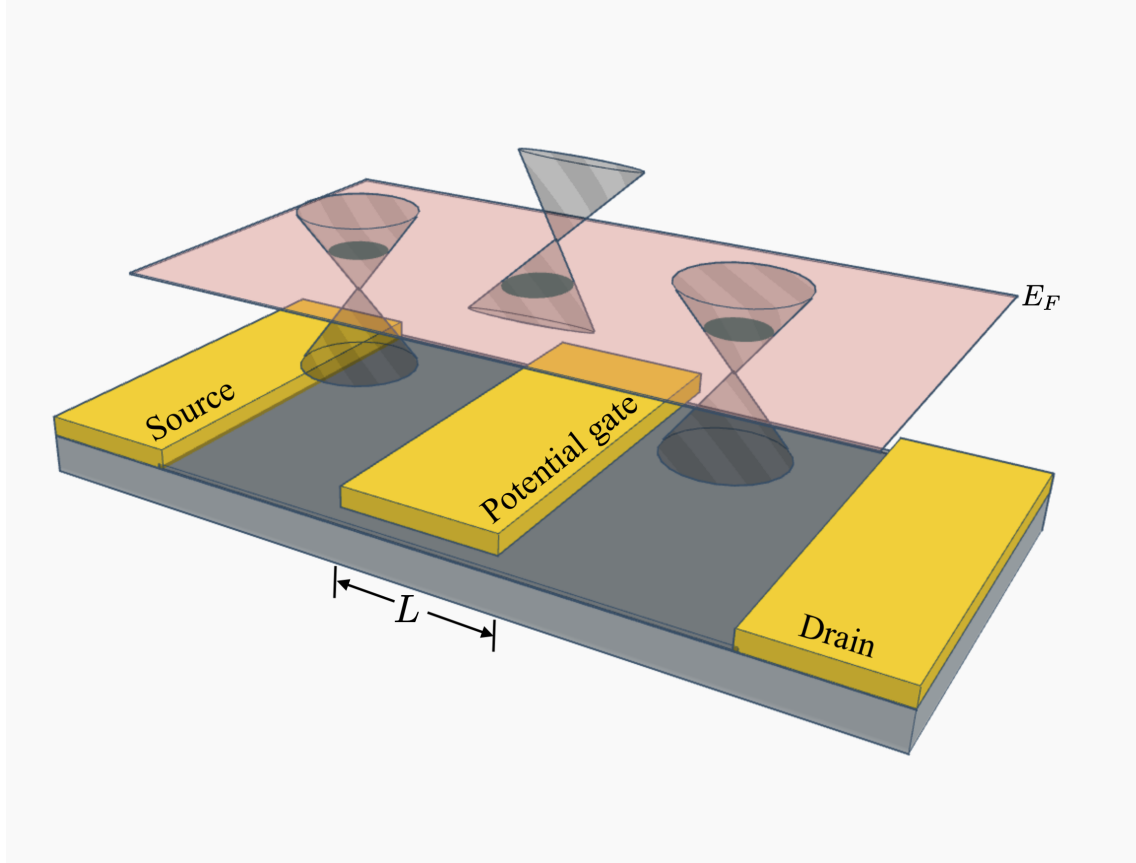


**Figure 3.1** Schematic illustration of Dirac material n-p-n heterojunctions with the mismatch of Dirac cone. The position of Fermi energy level  $E_F$  can be controlled by tuning the voltage through potential gate of length  $L$ .

### 3.2 Transmission probability of electron in tilted Dirac cone

The wave function of Dirac electron in general Dirac materials can be obtain by solving the eigenvalue problem. Since the low-energy quasiparticles in Dirac material mimic relativistic particle, it can be described by effective massless Dirac Hamiltonian

$$\hat{H} = \hbar(v_F\sigma \cdot k + w\sigma_0 \cdot k) + U\sigma_0 \quad (3.1)$$

where  $U$  is barrier height,  $v_F = 10^6 \text{ ms}^{-1}$  is Fermi velocity,  $k = (k_x, k_y)$  is wave vector in the x-y plane,  $\sigma = (\sigma_x, \sigma_y)$  is Pauli matrices,  $\sigma_0$  is a  $2 \times 2$  identity matrix, and  $w = (w_x, w_y)$  is the parameter with the dimension of velocity denoting the tilt of Dirac cone. By solving Eq. 3.1, we obtain the wave function for each region as

follows

$$\begin{aligned}\psi_1 &= \begin{cases} e^{ik_x x} + r e^{-ik_x x} & , x < 0 \\ s(e^{ik_x x} e^{i\phi} + r e^{-ik_x x} e^{-i\phi}) & , x < 0 \end{cases} \\ \psi_2 &= \begin{cases} a e^{iq_x x} + b e^{-iq_x x} & , 0 \leq x < L \\ s'(a e^{iq_x x} e^{i\theta} - b e^{-iq_x x} e^{-i\theta}) & , 0 \leq x < L \end{cases} \\ \psi_3 &= \begin{cases} t e^{ik_x x} & , x \geq L \\ s t e^{ik_x x} e^{i\phi} & , x \geq L \end{cases}\end{aligned}\quad (3.2)$$

The transmission coefficient  $t$  can be obtained by considering the continuity of the wave function at the boundaries  $x = 0$  and  $x = L$

$$\begin{aligned}-a - b + r &= -1 \\ -s r e^{-i\phi} - s' (a e^{i\theta} - b e^{-i\theta}) &= -s e^{i\phi} \\ a e^{iL q_x} + b e^{-iL q_x} - t e^{i k_x L} &= 0 \\ s' (a e^{i\theta+iL q_x} - b e^{-i\theta-iL q_x}) - s t e^{i k_x L+i\phi} &= 0\end{aligned}\quad (3.3)$$

It is easier to solve for  $t$  using Cramer's rule. First put Eq. 3.3 into a matrix form, where each column from left to right contain the factor of the coefficient  $r, a, b$ , and  $t$  respectively.

$$M_1 = \begin{pmatrix} 1 & -1 & -1 & 0 \\ -s e^{-i\phi} & -s' e^{i\theta} & e^{-i\theta} s' & 0 \\ 0 & e^{iL q_x} & e^{-iL q_x} & -t e^{i k_x L} \\ 0 & s' e^{i\theta+iL q_x} & -s' e^{-i\theta-iL q_x} & -s t e^{i k_x L+i\phi} \end{pmatrix} \quad (3.4)$$

Then, replace the column  $t$  with the factor on the right hand side of Eq. 3.3

$$M_2 = \begin{pmatrix} 1 & -1 & -1 & -1 \\ -s e^{-i\phi} & -s' e^{i\theta} & e^{-i\theta} s' & -s e^{i\phi} \\ 0 & e^{iL q_x} & e^{-iL q_x} & 0 \\ 0 & s_p e^{i\theta+iL q_x} & -s' e^{-i\theta-iL q_x} & 0 \end{pmatrix} \quad (3.5)$$

The transmission coefficient  $t$  can be obtain from  $t = \det M_2 / \det M_1$

$$t = \frac{2 s s' \cos(\theta) \cos(\phi) (\sin(k_x L) + i \cos(k_x L))}{\sin(L q_x) (s^2 - 2 s s' \sin(\theta) \sin(\phi) + s'^2) + 2 i s s' \cos(\theta) \cos(\phi) \cos(L q_x)} \quad (3.6)$$

The transmission probability can be obtained from  $T = t^* t$

$$T = \frac{\cos^2 \theta \cos^2 \phi}{\cos^2(L q_x) \cos^2 \theta \cos^2 \phi + \sin^2(L q_x) (1 - s s' \sin \theta \sin \phi)^2} \quad (3.7)$$

### 3.3 The elliptic Fermi surface of tilted Dirac cone

When the Dirac cone is tilted, we obtain the elliptic Fermi surface in which the wavevector of electron is directional-dependent. To understand relation between the electron wavevector and its incident angle  $\phi$ , we consider the elliptic equation with the major axis of the ellipse is in y-direction.

$$\frac{k_x^2}{k_a^2} + \frac{k_y^2}{k_b^2} = 1 \quad (3.8)$$

where  $k_x = k \cos \phi$  and  $k_y = k \sin \phi + k_c$ . Multiply both side with  $k_a^2 k_b^2$  and substituting  $\cos^2 \phi = 1 - \sin^2 \phi$

$$k_b^2 k^2 - k_b^2 k^2 \sin^2 \phi + k_a^2 k^2 \sin^2 \phi + 2k_a^2 k c \sin \phi + k_a^2 c^2) = k_a^2 k_b^2$$

Since  $k_a = k_b \sqrt{1 - w_0^2}$  and  $k_c = k_b w_0$  where  $w_0$  is eccentricity of the ellipse, we obtain

$$k_b^2 k^2 - k_b^2 k^2 \sin^2 \phi + k_b^2 (1 - w_0^2) k^2 \sin^2 \phi + 2k_b^2 (1 - w_0^2) k k_b w_0 \sin \phi + k_b^2 (1 - w_0^2) k_b^2 w_0^2 = k_b^2 (1 - w_0^2) k_b^2$$

Multiplying both side with  $-1/k_b^2$  and rearranging, we obtain

$$k = \pm(k w_0 \sin \phi - k_b (1 - w_0^2)) \quad (3.9)$$

Since  $k$  is nonnegative, we have to choose the solution such that  $k$  is positive.

Consider the case where  $w_0 = 0$

$$k = \pm(-k_b)$$

We choose the negative solution in order for  $k$  to be positive.

$$\begin{aligned} k &= -k w_0 \sin \phi + k_b (1 - w_0^2) \\ k &= \frac{k_b (1 - w_0^2)}{1 + w_0 \sin \phi} \end{aligned} \quad (3.10)$$

### 3.4 Angular dependent wavevector of tilted Dirac cone

We assume that the Dirac cone only tilted in y-direction. Therefore, the corresponding eigenenergy of Eq. 3.1 can be written as,

$$E_\eta = \hbar(\eta \sqrt{k_x^2 v_x^2 + k_y^2 v_y^2} + k_y w_y) + U \quad (3.11)$$

where  $\eta$  is band index. Since the tilt of Dirac cone determines the shape of Fermi surface in which the wave vector  $k$  is directional dependent. In order to see the form of wave vector under the effect of tilted Dirac cone, Eq. 3.11 can be rearranged to elliptic form

$$\frac{k_x^2}{k_a^2} + \frac{(k_y + k_c)^2}{k_b^2} = 1 \quad (3.12)$$

where

$$k_a = \frac{(E_F - U)^2 v_y^2}{\hbar^2 (\eta^2 v_y^2 - w_y^2) v_x^2}, k_b = \frac{\eta^2 v_y^2 (E_F - U)^2}{\hbar^2 (\eta^2 v_y^2 - w_y^2)^2}, k_c = \frac{(E_F - U) w_y}{\hbar (\eta^2 v_y^2 - w_y^2)}$$

We have, in section 3.3, introduced the wavevector of electron as a function of incident angle. We can substitute  $k_b$  and  $k_c$  to Eq. 3.10, which gives

$$k = \frac{k_b(1 - w_0^2)}{1 + w_0 \sin \phi} = \frac{E_F - U}{\eta \hbar v_F (1 + w_0 \sin \phi)} \quad (3.13)$$

where  $w_0$  here in this case is called tilted parameter.

## CHAPTER 4 RESULT AND DISCUSSION

We start by investigating the tunneling properties of electron across tilted Dirac cone heterojunctions where we focus on how the effect of the gate potential and tilt affect the electron transmission. Then, we demonstrate a method to measure the tilted strength of the Dirac cone by identifying the tunneling behavior. Finally, we show that the transport behaviors of electron in tilted Dirac cone material are analogous to electron under the influence of magnetic field. We also show the derivation of magnetic field strength as a function of gate potential and tilted parameter.

The calculation of transmission probability is carried out using Eq. 3.7

### 4.1 Angular dependent of transmission probability

The transmission probabilities across the tilted Dirac cone heterojunctions under the variation of gate potential are presented in Fig. 4.1. The transmission profiles are symmetric in the case of  $w_0 = 0$  regardless of the gate potential. When the tilted parameter is non-zero, the transmission profiles are shifted along the direction of the tilt and consequently become asymmetric, where the magnitude of the shift depends on the tilted strength of the Dirac cone. However, the present of the tilt barely affects the tunneling profiles when the applied gate potential is close to the Fermi energy as shown in Fig. 4.1b. This is because the Fermi surface is small and the allowed wavevector states are narrowed. Therefore, electron propagations other than the normal incident are backscattered.

Interestingly, when the applied gate voltage  $U$  is larger than the Fermi energy  $E_F$ , the transmission profiles exhibit peak tunneling as shown in Fig. 4.1c-d. These kind of tunnelings are called resonant tunneling, which occurred when the condition  $q_x L = n\pi$ ,  $n = 0, \pm 1, \dots$  in Eq. 3.7 is met.

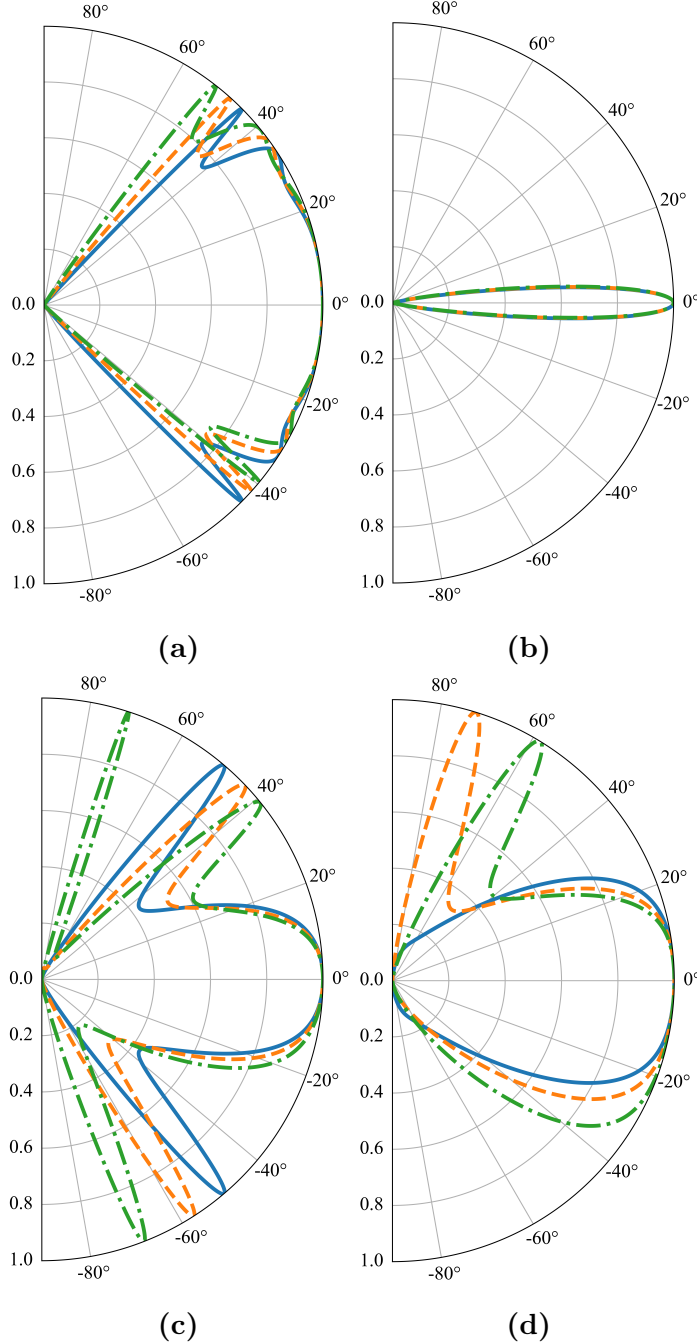


**Figure 4.1** The same cup of coffee. Two times.

## 4.2 The tilted strength identification by means of the tunneling resonance properties

The resonant tunnelings are arisen if the given  $U, E_F$  and,  $w_0$  satisfy the resonance condition. Modulating these parameters result in shifting of resonant tunneling angles as previously reported in section 4.1. In this section, we demonstrate that by measuring the asymmetric resonant tunneling angles, the tilted parameter can be

determined. Consider the resonance condition

$$\begin{aligned} L \sqrt{\left( \frac{E_F - U}{\hbar v_F} + w_0 k_y \right)^2 - k_y^2} &= n\pi \\ w_{0\pm} &= \frac{U - E_F}{\hbar v_F k \sin \phi} \mp \sqrt{1 + \left( \frac{n\pi}{kL \sin \phi} \right)^2} \end{aligned} \quad (4.1)$$

where subscript  $+(-)$  satisfy the positive(negative) angle  $\phi$  region. One can obtain the tilted parameter by applying the gate voltage and Fermi energy then measure the resonant tunneling angle, which can be experimentally observed by four-point probes technique [7]. To illustrate how to calculate for the tilted parameter, we substitute the configuration of dashed-dotted line in Fig. 4.1c to Eq. 4.1. We choose the resonance condition  $n = 4$ , which corresponds to the resonant tunneling angle  $\phi = 72^\circ$ . We find  $w_0 = 0.1$ .

However, this method is not at all practical since the variable  $n$  is unlikely observable. Also, the only way to manipulate the electron propagations is by tuning the voltages through the bottom and top gate. In section 4.4, we propose a more practical method to identify the tilted strength, which again, involve with the resonant tunneling behaviors.

### 4.3 Oscillatory behavior of electron resonant tunneling

To understand the behaviors of resonant tunneling under the effect of the tilt and gate potential, we plot the transmission probabilities at particular incident angle  $\phi = 45^\circ$  shown in Fig. 4.2. We found that the resonant tunneling oscillate with the increasing of gate voltage where the voltage difference between each resonance condition is the same. Also The voltages required to satisfy the resonance conditions are increased with the tilted strength. These resonant tunnelings are shifted uniformly with the tilted parameter, which can be confirmed mathematically by taking the derivative to Eq. 4.1 with respect to  $U$

$$\begin{aligned} \frac{dw_{0\pm}}{dU} &= \frac{d}{dU} \left( \frac{U - E_F}{\hbar v_F k \sin \phi} \mp \sqrt{1 + \left( \frac{n\pi}{kL \sin \phi} \right)^2} \right) \\ &= \frac{1}{\hbar v_F k \sin \phi}. \end{aligned} \quad (4.2)$$

Eq. 4.2 indicates that the tilted parameter is linearly proportional to gate voltage.

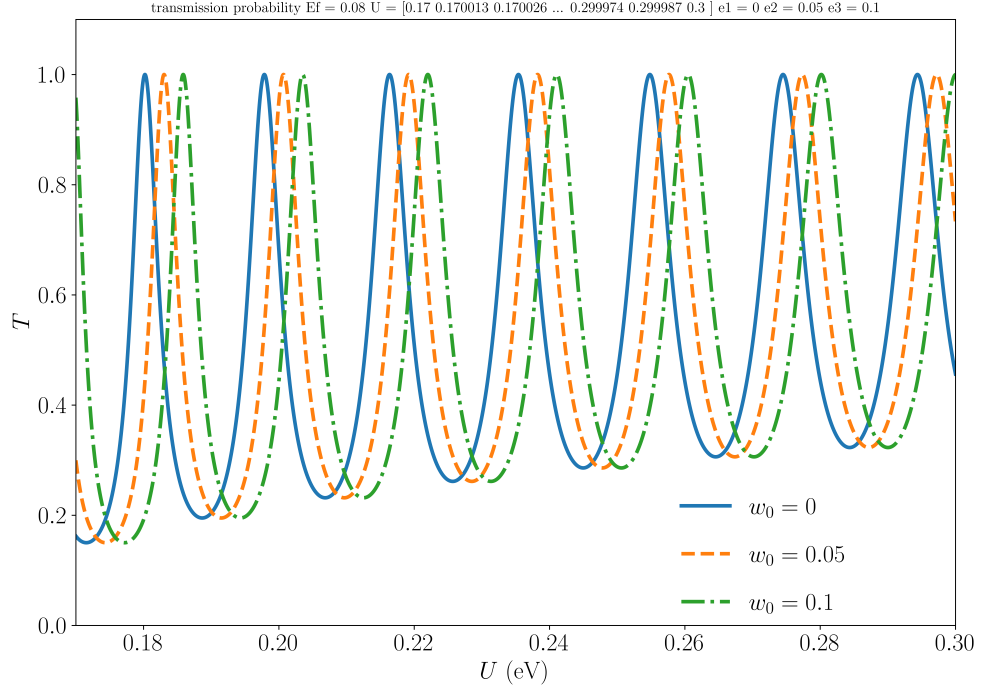


**Figure 4.2** tp fixed angle

#### 4.4 Revisit: The tilted strength identification by means of the tunneling resonance properties

In section 4.2, we have demonstrated a method to identify the character of Dirac cone using the resonant tunneling properties. The method can be applied to any resonance condition given that we have known its corresponding resonant tunneling angle. However, it is still not a practical method since the parameter  $n$  is unobservable. Also, most device configurations have fixed angled probes to observe the resonant tunneling current. In this section, we revisit this study again and eliminate the drawbacks mentioned above.

We have discussed earlier in section 4.3 that the relation of  $w_0$  and  $U$  are linear with the slope of  $1/\hbar v_F k \sin \phi$ . For this reason, we can identify the tilted strength by measuring the difference between two voltages satisfied the same resonance con-

dition.

$$\Delta w = \frac{\Delta U}{\hbar v_F k_y} \quad (4.3)$$

To apply Eq. 4.3 to determine the tilted parameter, the voltages satisfied the same resonance condition have to be first determined, which can be achieved using the device structure depicted in Fig. 4.3a. We have to tune  $U$  until the resonant tunneling occurs at  $\phi = \pi/4$ , where the electron current can be measured as shown in Fig. 4.3b. The voltage at which the resonant tunneling occurs at  $\phi = \pi/4$  for the case of non-tilted Dirac cone can be easily obtained since it is the system found in pristine graphene. Substituting these gate voltages to Eq. 4.3 we obtain  $w_0 = 0.1$

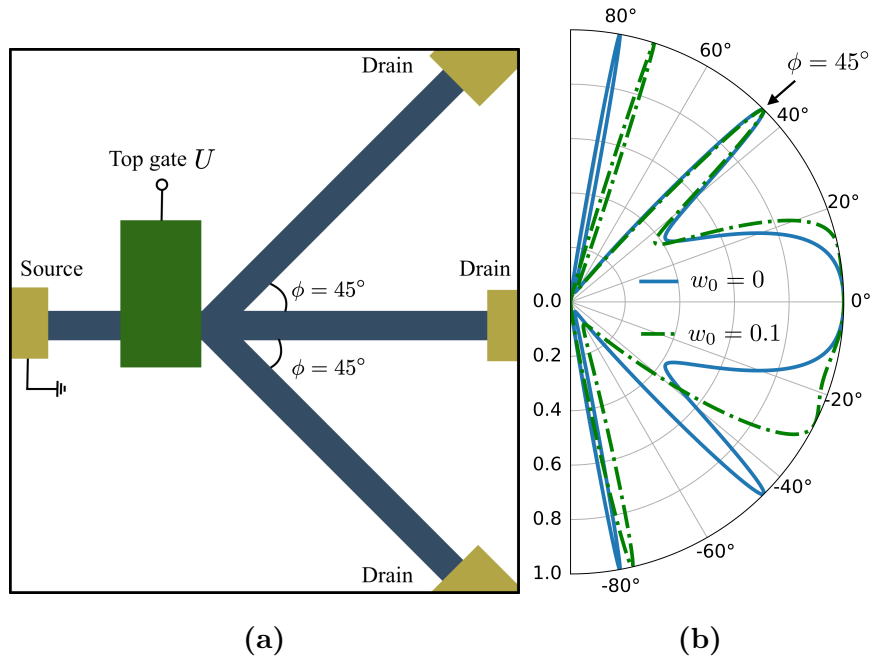


**Figure 4.3** (a) The device structure for the measurement of resonant tunneling electron. Straight blue lines represent the transport region where both arms are  $45^\circ$  angled with the normal direction. Green and yellow region represents top gate and electrode respectively. (b) Angular-dependent transmission for different applied voltages,  $U=180.2$  meV for solid line and  $U=185.85$  meV for dashed-dotted line. These voltages satisfy the resonance condition at  $\phi = \frac{\pi}{4}$ .

## 4.5 Pseudo magnetic field

In section 4.1, we have shown that the tunneling behavior of electron across the tilted Dirac cone exhibits asymmetric transmission. Previously, the transmission of this kind can be achieved by applying the magnetic barrier to the system [8, 9]. In this section, we demonstrate that the similar transmission profile can also be achieved in the tilted Dirac cone system without the magnetic barrier. Consider the x-component wavevector inside the barrier region  $q_x = \sqrt{q^2 - k_y^2}$ , which can be rearranged into the form

$$q_x \approx \sqrt{q'^2 - (k_y - q'w_0)^2} \quad (4.4)$$

where  $q' = \frac{E_F - U}{\eta \hbar v_F}$ . Notice that the y-component wavevector in Eq. 4.4 is shifted by the tilted Dirac cone similar to the wavevector shift by the effect of magnetic vector potential. Based on this analogy, we can derive the equivalent pseudo magnetic field

$$\begin{aligned} -q'w_0 &= \frac{\xi}{l_B} \\ -\left(\frac{E_F - U}{\eta \hbar v_F}\right) w_0 &= \xi \sqrt{\frac{|e|B}{\hbar}} \\ B &= \left(\frac{\varepsilon w_0}{v_F}\right)^2 \frac{1}{\xi \gamma \hbar |e|} \end{aligned} \quad (4.5)$$

where  $\varepsilon = E_F - U$  is effective Fermi energy.  $\xi = \pm 1$  is in fact the direction of magnetic field, but since these fields are induced by the tilted Dirac cone, it can be considered as the direction of the tilt. The positive(negative) sign mean that the Dirac cone tilted to the left(right) side with respect to normal direction.  $\gamma = \pm 1$  indicate the carrier type in Fermi energy level.

## 4.6 The key consequence of the mismatch effect

We have found in section 4.5 that both the potential and tilt are the source of pseudo-magnetic field effect, where the strength and direction of the field can be controlled by tuning the effective Fermi energy. This effect actually been proposed in Weyl semimetal n-p-n junction with tilted Weyl cones [11]. However, the coupling of the tilt and top gate potential barrier is required to preserve the effect. In contrast to our work, where the top gate potential can be set to zero, and pseudo-magnetic field effect still occurred according to Eq. 4.5. Which is the consequence of the

existence of the mismatch between Dirac cones with different tilted parameters. To show how the mismatch plays an important role in mimicking the pseudo-magnetic field effect without the requirement of potential barrier. We sketch the Fermi surface of the first and second regions, as shown in Fig. 4.4a, where top gate potential is set to zero. Hence, electrons in both regions occupy in the same Fermi energy level. If the Dirac cones are tilted homogeneously, the Fermi surface of both regions are completely overlapped. Consequently, the electron can symmetrically propagate in all directions as shown in Fig. 4.4b. When the inhomogeneity is introduced, where only the Dirac cone in the second region is tilted while the first region is vertical non-tilted. The Fermi surfaces are partially overlapping as indicated by shaded area, which lead to asymmetric tunneling.

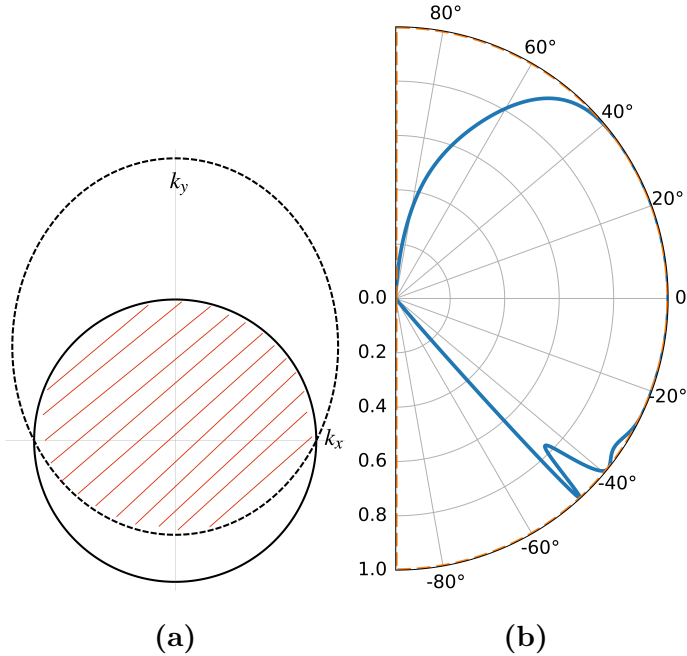


**Figure 4.4** (a) The Fermi surfaces of Dirac cones in different regions. The solid line represents the Fermi surface of non-tilted Dirac cone in region I and the dashed line represents the Fermi surface of tilted Dirac cone  $w_0 = 0.5$  in region II. (b) The transmission probabilities as a function of incident angle, where the solid (dashed) line is the case of the system with (without) the mismatch of Dirac cones. The Fermi energy  $E_F = 80$  meV and gate potential is zero.

## 4.7 Transmission under the influence of pseudo magnetic field

To illustrate how pseudo magnetic field affects the tunneling behaviors compared to their real counterpart, the transmissions under the effect of pseudo and real magnetic fields are plotted as shown in Fig.4.5. First consider the case  $U \gg E_F$ , we found that when the tilted parameter is small, the transmission profiles between the two systems are almost identical, as shown in Fig. 4.5a, which confirms the existence of pseudo-MVP. However, the pseudo-MVP is valid only if the strength of the tilt is small. Otherwise, the transmission profiles would become distinguishable, as shown in Fig. 4.5b. The same applies in the case of potential barrier  $U = 0$ , where the pseudo-MVP occurs when  $w_0$  is small and becomes weak as  $w_0$  increase as shown in Fig. 4.5c-d.

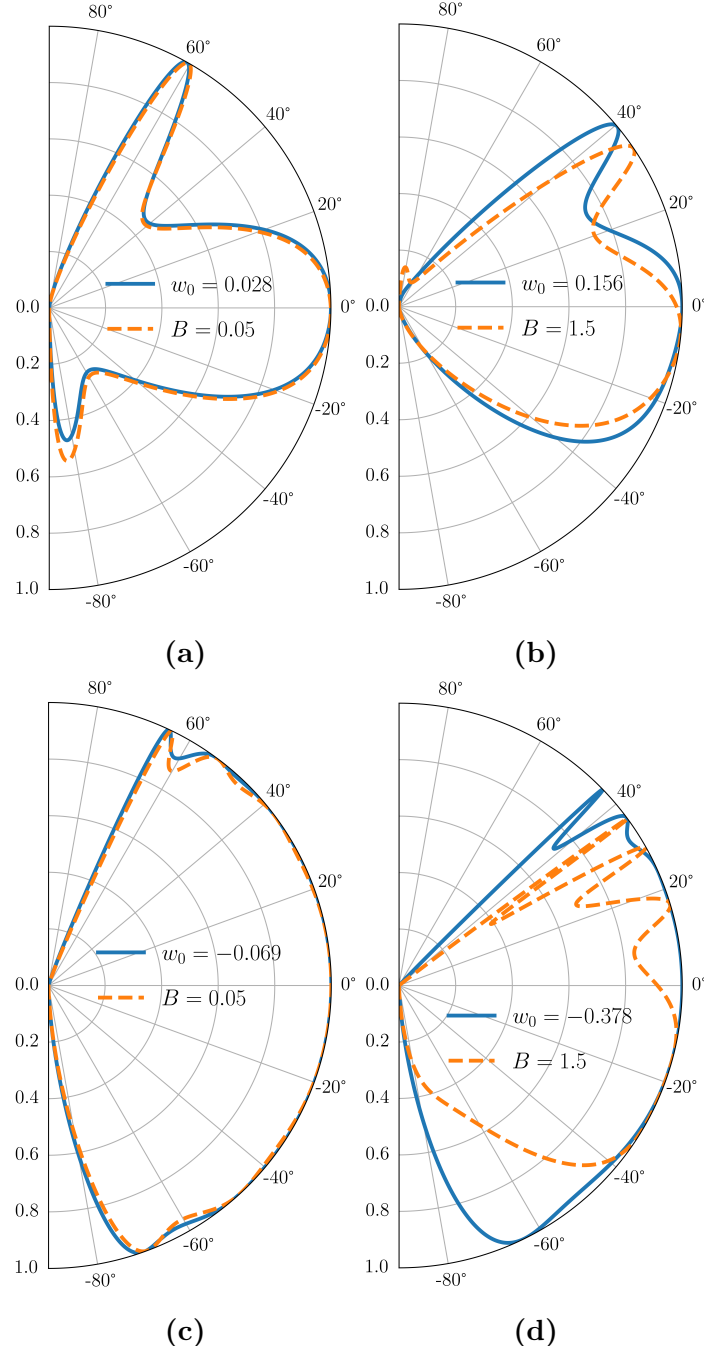


**Figure 4.5** The polar plot of transmission probabilities as a function of incident angle of the system with tilted mismatch Dirac cone (solid line) and non-tilted system under the influence of delta magnetic field (dashed line). The Fermi energy  $E_F = 83$  meV is the same for all plot, the gate potential  $U = 285$  meV for (a) and (b),  $U = 0$  for (c) and (d)

## **CHAPTER 5 CONCLUSION**

The transmission probabilities of electron across tilted Dirac cone undergo the effect of pseudo magnetic field

## REFERENCES

1. D. S.L. Abergel and Tapash Chakraborty, “Generation of valley polarized current in bilayer graphene,” **Applied Physics Letters**, vol. 95, no. 6, pp. 10–13, 2009.
2. T. Fujita, M. B.A. Jalil, and S. G. Tan, “Valley filter in strain engineered graphene,” **Applied Physics Letters**, vol. 97, no. 4, pp. 2012–2015, 2010.
3. B. Huard, J. A. Sulpizio, N. Stander, K. Todd, B. Yang, and D. Goldhaber-Gordon, “Transport measurements across a tunable potential barrier in graphene,” **Physical Review Letters**, vol. 98, no. 23, pp. 8–11, 2007.
4. M. I. Katsnelson, K. S. Novoselov, and A. K. Geim, “Chiral tunnelling and the Klein paradox in graphene,” **Nature Physics**, vol. 2, no. 9, pp. 620–625, 2006.
5. Vitor M. Pereira and A. H. Castro Neto, “Strain Engineering of Graphene’s Electronic Structure,” **Physical Review Letters**, vol. 103, no. 4, pp. 1–4, 2009.
6. Meeghage Madusanka Perera, Ming Wei Lin, Hsun Jen Chuang, Bhim Prasad Chamlagain, Chongyu Wang, Xuebin Tan, Mark Ming Cheng Cheng, David Tománek, and Zhixian Zhou, “Improved carrier mobility in few-layer MoS<sub>2</sub> field-effect transistors with ionic-liquid gating,” **ACS Nano**, vol. 7, no. 5, pp. 4449–4458, 2013.
7. Atikur Rahman, Janice Wynn Guikema, Nora M. Hassan, and Nina Marković, “Angle-dependent transmission in graphene heterojunctions,” **Applied Physics Letters**, vol. 106, no. 1, 2015.
8. M. Ramezani Masir, P. Vasilopoulos, A. Matulis, and F. M. Peeters, “Direction-dependent tunneling through nanostructured magnetic barriers in graphene,” **Physical Review B - Condensed Matter and Materials Physics**, vol. 77, no. 23, pp. 1–11, 2008.

9. M. Ramezani Masir, P. Vasilopoulos, and F. M. Peeters, “Fabry-Pérot resonances in graphene microstructures: Influence of a magnetic field,” **Physical Review B - Condensed Matter and Materials Physics**, vol. 82, no. 11, pp. 1–12, 2010.
10. Zhenhua Wu, F. M. Peeters, and Kai Chang, “Electron tunneling through double magnetic barriers on the surface of a topological insulator,” **Physical Review B - Condensed Matter and Materials Physics**, vol. 82, no. 11, pp. 1–7, 2010.
11. Can Yesilyurt, Zhuo Bin Siu, Seng Ghee Tan, Gengchiau Liang, Shengyuan A. Yang, and Mansoor B.A. Jalil, “Anomalous tunneling characteristic of Weyl semimetals with tilted energy dispersion,” **Applied Physics Letters**, vol. 111, no. 6, 2017.

# CURRICULUM VITAE

**NAME** Mr. Eakkarat Pattrawutthiwong

**DATE OF BIRTH** 26 April 1995

## EDUCATIONAL RECORD

HIGH SCHOOL	High School Graduation Kaen Nakhon Wittayalai School, 2014
BACHELOR'S DEGREE	Bachelor of Science (Applied Physics) King Mongkut's University of Technology Thonburi, 2018
MASTER'S DEGREE	Master of Science (Physics) King Mongkut's University of Technology Thonburi, 2020
PUBLICATION	Soodchomshom, B., Niyomsoot, K., Pattrawutthiwong, E, "Switching effects and spin-valley Andreev resonant peak shifting in silicene superconductor," <b>Physica E: Low-dimensional Systems and Nanostructures</b> , vol 97, pp. 375-383, 2018